Case Studies in Thermal Engineering 31 (2022) 101843

Contents lists available at ScienceDirect

Case Studies in Thermal Engineering

journal homepage: www.elsevier.com/locate/csite

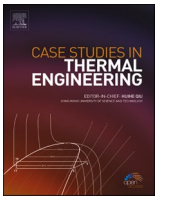

Microwave imaging of breast cancer: Simulation analysis of SAR and temperature in tumors for different age and type

Deepshikha Bhargava, Phadungsak Rattanadecho *

Department of Mechanical Engineering, Faculty of Engineering, Thammasat University, Rangsit Campus, 99 moo 18, Khlong Luang, Pathum Thani, 12120, Thailand

ARTICLE INFO

Keywords:
Breast cancer detection
Microstrip patch antenna
Confocal microwave imaging
SAR
Temperature

ABSTRACT

Microwave imaging (MI) offers a safer, cheaper, and an effective way of detecting breast cancer. In this analysis, a wide-band microstrip patch antenna working between 3.6 to 9.2 GHz frequency range has been used in a monostatic MI system for breast cancer detection. A breast model made of skin, fat and tumor is exposed to the antenna radiation. The antenna scans the breast model at 77 positions and collects the reflection coefficients from each scan. Confocal Microwave Imaging (CMI) algorithm is used on those collected reflection coefficients to generate a 2D image of the breast. This 2D image of the breast shows the presence of the tumor inside it. SAR in the breast layers for dielectric properties of the tumor based on different age group (47, 49, 51, and 45) and types are calculated. Temperature in the breast layers are also calculated in the presence of the cancerous tumor and found to be correlated with the SAR. The results show a significant increase in the SAR and temperature in the breast layers in presence of the tumor. Moreover, SAR and temperature increase seem to be highly dependent on the dielectric and thermal properties of the breast layers.

1. Introduction

Breast cancer has become a major reason of death in women around the world [1]. Early detection of these cancerous cells is crucial as it is the only way of providing a rapid and correct treatment. Over the years, there have been several techniques used for detecting the breast cancer. Among them, the most popular are X-ray mammography, ultrasound, and magnetic resonance imaging (MRI). These techniques, however, suffers from some serious inherent disadvantages. X-ray mammography uses non-ionizing radiations which, if used for longer time, can cause adverse effect on patient's health. Also, some women might find the procedure uncomfortable as X-ray mammography requires the breast to be pressed in between the mammography equipment. It is expensive and not easily accessible [2,3]. In comparison to X-ray mammography, ultrasound and MRI are safer alternatives as both the techniques use non-ionizing radiation. However, these are less effective and mostly used at the later stages of the breast imaging to distinguish between the cancerous and non-cancerous cells [4,5]. Even all aforementioned techniques used in combination cannot satisfy the requirement of the U.S. Institute of Medicine reported in Ref. [6].

The fact that cancerous and non-cancerous cells, at microwave frequencies, possess a notable contrast in their dielectric properties has attracted researchers' interest recently. Giving birth to a promising and a potential technique known as microwave imaging (MI). MI is a non-invasive, non-ionizing, and an inexpensive technique [7]. It works under the microwave frequency range and does not

* Corresponding author.
E-mail address: ratphadu@engr.tu.ac.th (P. Rattanadecho).

https://doi.org/10.1016/j.csite.2022.101843
Received 12 April 2021; Received in revised form 28 January 2022; Accepted 1 February 2022
Available online 4 February 2022

require the breasts to be compressed in between the equipment. In MI, the microwave signals irradiate the breast tissue from outside at several points. When microwave interact with the breast tissue some part of it gets transmitted where some gets reflected back. The signals that get reflected back, also known as scattered signals, are stored and processed through an imaging algorithm to generate a 2D image of the breast. This resultant image of the breast shows the presence of the tumor inside it [3,8,9]. There are mainly two types of MI techniques. Tomography and radar-based. In tomography, a whole dielectric image of the breast is created from the scattered signals by using an ill-posed inverse scattering approach [10,11]. This technique is complex and time-consuming. In radar-based MI, however, the stored scattered signals are processed using an effective algorithm to generate a 2D image of the breast region containing the tumor.

In radar-based microwave imaging, antennas are used to scan the breast at several points. Because of the difference found in the dielectric properties of the healthy and cancerous tissues, the scattered signals reflected from a healthy tissue shows a huge contrast from the cancerous tissue. This difference in the scattered signals are the key in radar-based MI [12,13]. The radar-based MI is of three types: monostatic, bi-static, and multi-static. In monostatic MI, only one antenna is used as both a transmitter and as well as a receiver. In bi-static MI, two antennas are used, one working as a transmitter and other as a receiver. Whereas, in multi-static MI, an array of antenna is used. One antenna, at one time, working as a transmitter while others as receivers. Patch antennas due to their low cost, easy fabrication, and ease of accessibility are widely used in radar-based MI [14–16]. However, these antennas suffer from narrow band-width. For a good resolution range, a wide band-width is preferable. So, in order to make the patch antenna wideband several techniques are used [17,18], among them adding slots and performing parametric analysis is one of the simplest and cheapest technique [14,19].

The dielectric difference found in the healthy and cancerous tissues not only produces difference in the reflection coefficients but also shows difference in the way they absorb those incident microwave radiation. The absorption of EM radiation by tissues is measured in SAR (specific absorption rate). In our previous work, we have extensively studied the measurement of SAR in different layers of human tissues. It has been observed that SAR highly depends on the tissue's dielectric properties [20–22]. In cancerous tumor, absorption of EM radiation is very different than the other surrounding tissues [23,24]. This difference found in the SAR can also be used as a key to determine the position and type of the tumor inside the tissues. The absorbed EM radiation in the tissue then converts into heat which increases the temperature within the tissues. The temperature in the tumor, just like SAR, would also be very different than the other tissues of the breast. This could also be useful for tumor detection purpose.

Moreover, cancerous tumor in different age group of women has a notable difference in their dielectric properties. A normal, benign, and cancerous tumor all together have a notable difference in their dielectric properties measured at the same frequencies. To see how the EM radiation absorption in different age group of women and in different types of tumors differ from each other can also be an interesting analysis to conduct.

Hence, this study proposes a monostatic radar-based MI system for breast cancer detection. A model of three layers of breast tissues and a microstrip patch antenna is used in the MI system as shown in Fig. 1. The antenna is working both as a transmitter and a receiver. The reflected signals are stored and a confocal microwave imaging algorithm is applied on the signals to generate a 2D image of the breast showing the position of the cancerous tumor in it. Different size of tumors at different distances were placed to test the capability of the proposed antenna in detecting them. Coupled model of EM wave propagation and bioheat transfer is solved by using Finite Element Method (FEM). Maxwell equations are used to calculate the absorbed EM wave and Pennes' bioheat equation for the temperature increase in the tissues. SAR in the breast tissue in different age group of patients and different types of tumors is studied. Temperature increase in the breast due to the heat generation by the EM absorption is studied.

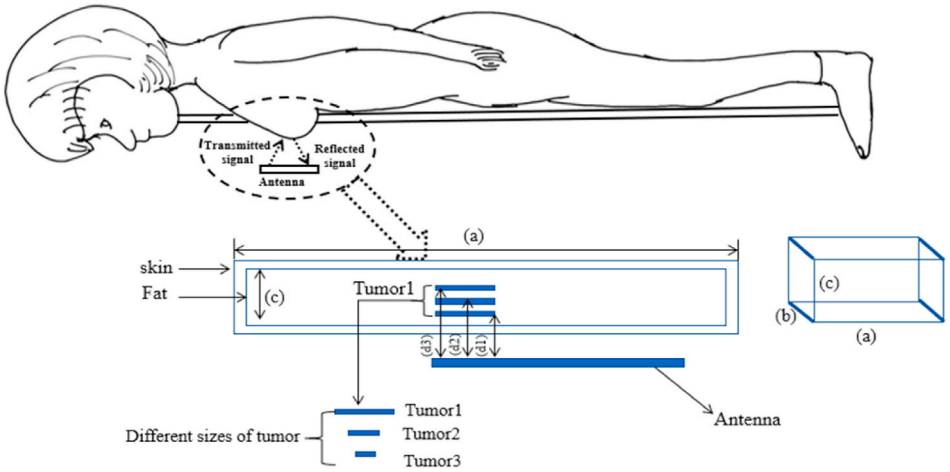

Fig. 1. Monostatic radar-based MI system for breast cancer detection.

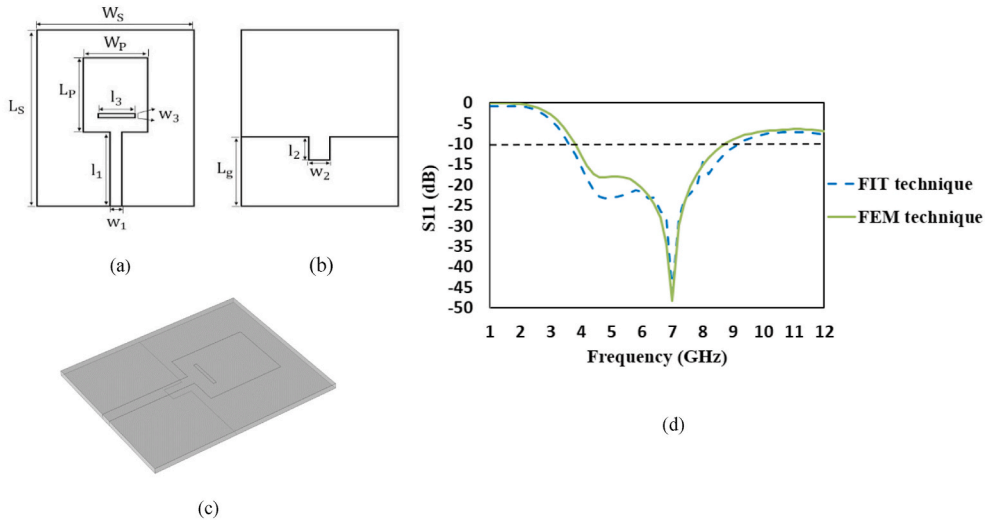

Fig. 2. Proposed antenna's: (a) front view, (b) back view, (c) 3-D view, and (d) Comparison with the simulated reflection coefficients (S11) in FIT.

Table 1
Dimensions of the antenna.

Parameter	Dimension
L_s	30 mm
W_s	25 mm
L_P	12 mm
W_p	10 mm
L_g	13.2 mm
l_1	14 mm
w_1	1.8 mm
l_2	3 mm
w_2	2.4 mm
l_3	5 mm
w_3	0.5 mm

Table 2
Dimensions of skin and fat tissues of the breast.

Tissues	(a)	(b)	(c)
Skin	50 mm	40 mm	10 mm
Fat	45 mm	35 mm	9 mm

Table 3
Dimensions of the tumors.

Tumors	(a)	(b)	(c)
Tumor 1	10 mm	10 mm	2.4 mm
Tumor 2	8 mm	8 mm	2.4 mm
Tumor 3	6 mm	6 mm	2.4 mm

2. Problem formulation

2.1. Antenna and breast modeling

A microstrip patch antenna made of FR4 substrate of thickness 0.794 mm and dielectric constant $\varepsilon_r = 3.34$ is designed to be used in MI system, as shown in Fig. 2 (a)(b)(c). Slots in the ground and patch of the antenna are added later on to enhance its overall performance. All the dimensions for the antenna including the slots are given in Table 1. The resultant reflection coefficient (S11) from

Table 4
Distances of tumors from the antenna.

Distances	Distance between the tumor and antenna
d1	4.2 mm
d2	6.2 mm
d3	8.2 mm

Table 5
Dielectric properties for skin and fat tissues of the breast [26].

Tissues	ε_r	σ (S/m)
Skin	37.9	1.49
Fat	5.14	0.14
Tumor	50	1.20

Table 6
Dielectric properties for the cancerous tumor, based on women age [27,28].

Women ages	Normal		Cancerous	
	ε_r	σ (S/m)	ε_r	σ (S/m)
47 Years	20.43	3.12	32.31	3.52
49 years	18.85	2.71	38.73	4.12
51 years	24.98	3.25	40.1	4.31
45 years	19.5	2.64	30	3.34

Table 7
Dielectric properties of different types of tumors at different frequencies [29].

Tumors	4 GHz		6 GHz		8 GHz	
	ε_r	σ (S/m)	ε_r	σ (S/m)	ε_r	σ (S/m)
Normal	7.202 ± 0.428	0.758 ± 0.119	6.569 ± 0.332	0.930 ± 0.187	6.292 ± 0.291	1.006 ± 0.219
Benign	18.303 ± 1.814	1.669 ± 0.077	16.093 ± 2.214	2.139 ± 0.079	15.120 ± 2.423	2.346 ± 0.877
Cancerous	59.125 ± 1.802	6.774 ± 0.356	56.551 ± 1.664	8.487 ± 0.633	55.425 ± 1.623	9.242 ± 0.755

FEM technique is compared with the S11 of the same antenna model made via FIT technique, as shown in Fig. 2(d). Both the S11 show similar results which validates the proposed antenna design. For breast model, three rectangular boxes are designed acting as the skin, fat, and tumor of the breast (Fig. 1). Table 2 shows the dimensions of each layer of the breast model. For testing the antenna's capability of detecting the smaller size tumors, three sizes of tumors are inserted one by one at three different distances from the antenna while the antenna scans the breast tissue (Fig. 1). The size of the tumors and their distances from the antenna are shown in Tables 3 and 4, respectively. Dielectric properties of the breast layers are given in Table 5. Tumor's dielectric properties are chosen based on two parameters. First, the dielectric properties of normal and cancerous tumor for different age of women shown in Table 6. Second, the dielectric properties of normal, benign, and cancerous tumor at different frequencies, as shown in Table 7. For the thermal properties, however, there is not enough information based on the women's age. Hence, thermal properties of cancerous tumor, given in Ref. [25] Table 8, are chosen in the study. For MI, SAR, and temperature calculation, tumor size of Tumor 1 placed at distance d2 is used.

2.2. Confocal MI algorithm

Confocal MI algorithm is used to generate a 2D image of the breast. For that Tumor 1 (Table 3) placed at a distance d2 (Table 4), having the dielectric properties from Table 5 is used. The antenna scans over the breast tissue twice at 77 positions. First, in the presence and then again in the absence of the tumor. Fig. 3(a) shows the coordinates for the antenna positions when it scans the breast. The reflection coefficients from both the scanning are collected and imported into MATLAB where CMI algorithm is applied on them. Fig. 3(b) shows the step by step procedure from scanning to generating a 2D image of the breast. Whereas, Fig. 3(c) shows the flow chart of the steps involved in the CMI algorithm [3,30].

Table 8
Thermal properties for the breast model [20,25].

Tissues	ρ (kg/m^3)	k (W/m°C)	C (J/kg°C)	Q_{met} (W/m^3)	ω_b (1/s)
Skin	1125	0.42	3600	1620	0.02
Fat	916	0.25	3000	300	4.58×10^{-4}
Tumor	1050	0.48	3858	5000	0.0063

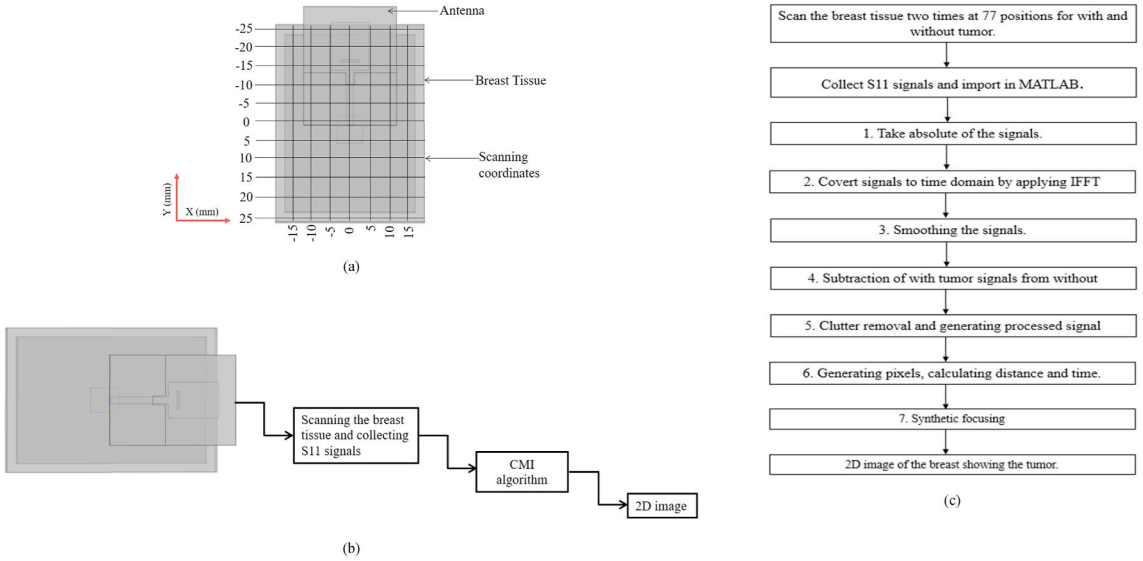

Fig. 3. CMI algorithm: (a) scanning coordinates of the antenna, (b) step by step procedure from breast scanning to 2D image, (c) steps involved in CMI algorithm.

1. Take absolute of the signals

The reflection coefficients (frequency domain) collected from both the cases are in negative values. Taking an absolute of those negative signals makes the further calculation easier. The reflection coefficient signals after taking an absolute are E_{XY} and EB_{XY} for the breast without tumor and breast with tumor, respectively.

2. Transformation

The frequency domain signals are then transformed to time domain signal by applying IFFT as shown in Equ. (1) and (2).

$$E_{XY}(t) = IFFT(E_{XY}) \tag{1}$$

$$EB_{XY}(t) = IFFT(EB_{XY}) \tag{2}$$

3. Smoothing

Savitzky-Golay filter (sgolay filter) is used to smooth the time domain signal to get a more continuous form of the signals, Eqs. (3) and (4)

$$E_{XYS}(t) = IFFT(E_{XY})*s \tag{3}$$

$$EB_{XYS}(t) = IFFT(EB_{XY})*s \tag{4}$$

4. Calibration

The time domain signal of breast with tumor is subtracted from the time domain signal of breast without tumor, Eq. (5). The signal after the subtraction has a higher peak which indicates the presence of the tumor.

$$C_{XYS}(t) = EB_{XYS}(t) - E_{XYS}(t) \tag{5}$$

5. Clutter removal

The $C_{XYS}(t)$ signal contains some reflection due to the antenna and environment [31]. To remove these reflections the calibrated signal is first averaged, Eq. (6), then subtracted from each signal, Eq. (7). Where N denotes number of antenna positions (77).

$$A_X(t) = \frac{\Sigma_{Y=1}^{N} C_{XYS}(t)}{N} \tag{6}$$

$$P_{XY}(t) = C_{XYS}(t) - A_X(t) \tag{7}$$

6. Synthetic focusing

Pixels in an area of 300 mm × 300 mm is considered where the distance from each antenna position (XY) to each pixel (x_i and y_j) is calculated. A monostatic MI is performed in the study, hence, distance from transmitter to pixel point and pixel point to receiver are same. Because of this the distance D_{XY} (x_i,y_j) is multiplied by 2, Eq. (8). Later, the round-trip time for the signal to reach back to the antenna is calculated, as shown in Equ. (9).

$$D_{XY}(x_i, y_j) = 2\sqrt{(X - x_i)^2 - (Y - y_j)^2 + d^2} \tag{8}$$

$$t_{XY}(x_i,\ y_j) = \frac{D_{XY}(x_i, y_j)}{c/\sqrt{\varepsilon_r}} \tag{9}$$

6. Image generation

Intensity value I (x_i,y_j) is calculated for each pixel point by evaluating the signal value of the processed signal $P_{XY}(t)$ at time t_{XY} (x_i, y_j), as represented in Equ. (10). Where r = total number of antenna position in row, c = total number of antenna position in column, I (x_i,y_j) = intensity value at pixel point (x_i, y_j).

$$I(x_i, y_j) = \left[\sum_{X=1}^{r}\sum_{Y=1}^{c} P_{XY}(t_{XY}(x_i, y_j))\right]^4 \tag{10}$$

2.3. Equations for electromagnetic wave propagation analysis

Simulation analysis is performed on a 3D model. To reduce the computational time and not to compromise with the accuracy of the results. Following assumptions have been made [20].

1. The EM radiation from the antenna propagates in free space in 3D.
2. The EM radiation gets in contact and interact with the breast model in an open domain.
3. The domain outside the breast model is truncated by applying SCB (scattering boundary conditions).
4. The dielectric properties of the breast model tissues remain same throughout the simulation.

Electromagnetic wave propagation around and in the breast model is solved by using Maxwell's equations, Equ. (11).

$$\nabla \times \frac{1}{\mu_r}\nabla \times \vec{E} - k_0^2 \varepsilon_r \vec{E} = 0 \tag{11}$$

$$\varepsilon_r = n^2$$

where $\vec{E}$ is electric field intensity (V/m), μ_r is relative magnetic permeability, ε_r is relative dielectric constant, and k_0 is the free space wave number (m^{-1}).

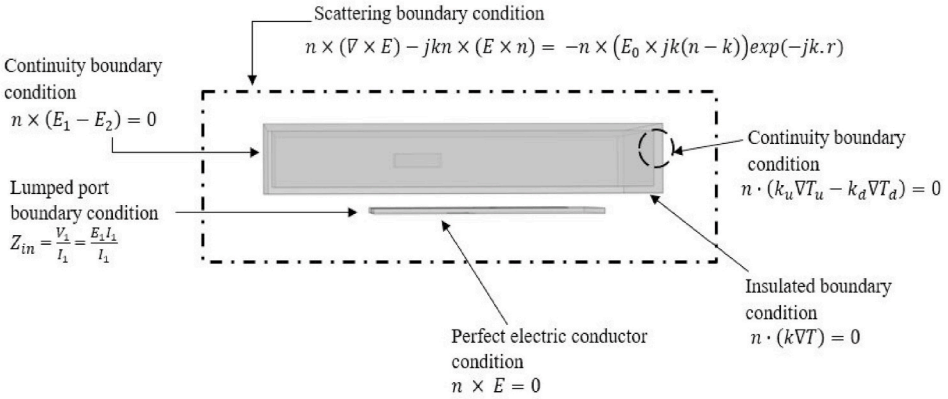

Fig. 4. Boundary condition for electromagnetic wave propagation and heat transfer analysis.

2.3.1. Boundary condition for wave propagation

A wide band microstrip patch antenna is used to generate microwaves. The bottom of the antenna connecting the microstrip line and ground plane is called lumped port Fig. 4, where voltage drop between the two planes is defined to give power to the patch antenna:

$$Z_{in} = \frac{V_1}{I_1} = \frac{\vec{E}_1 l_1}{I_1} \tag{12}$$

where Z_{in} is the input impedance (ohm), V_1 is the voltage along the edges, I_1 is the electric current magnitude (A), $\vec{E}_1$ is the electric field along the source edge (V/m) and l_1 is the edge length.

Continuity boundary condition are applied on the breast model interfaces such as between air and the breast layers (air, skin, fat):

$$n \times \left(\vec{E}_1 - \vec{E}_2\right) = 0 \tag{13}$$

In order to avoid the reflections occurring due to the interaction between the EM waves and the breast layers, a 3D PML (perfectly matched layer) are built around the breast model [32]. SCB are assigned on outer surface of the PML:

$$n \times \left(\nabla \times \vec{E}\right) - jkn \times \left(\vec{E} \times n\right) = -n \times \left(\vec{E}_0 \times jk(n-k)\right) exp(-jk.r) \tag{14}$$

where k is the wavenumber (m^{-1}), n is the normal vector, j = $\sqrt{-1}$, and $\vec{E}_0$ is the incident plane wave (V/m).

2.4. Interaction of electromagnetic waves with the breast tissues

The interaction of EM waves with the breast layers lead to energy absorption within the tissues. This absorbed energy is known as SAR (Specific Absorption Rate) which is expressed as the power dissipation rate normalized by the material density [33]:

$$\text{SAR} = \frac{\sigma}{\rho} \left|\vec{E}\right|^2 \tag{15}$$

where $\vec{E}$ is electric-field (V/m), σ is electric conductivity (S/m), and ρ is the tissue density (kg/ m^3).

2.5. Equation for heat transfer analysis

The temperature inside the breast layers has been calculated by using bioheat equation. The equation is consisting of the heat conduction, blood perfusion, and external heating. The initial temperature of the breast layers is set to 37 $^{\circ}C$. Again, to reduce the computation time following assumptions are made:

1. The thermal properties of the tissues stay same throughout the simulation.
2. The phase change of substances within the tissues are none.
3. The energy exchange within the breast model is none.
4. The chemical reactions of any type within the breast model are none.

Pennes' bioheat equation has been used to analyze the temperature distribution inside the breast layers [20,21,34]. Eq. (16) is a transient penne's bioheat equation describing the heat transfer in the breast layers:

$$\rho C \frac{\partial T}{\partial t} = \nabla \cdot (k \nabla T) + \rho_b C_b \omega_b (T_b - T) + Q_{met} + Q_{ext} \tag{16}$$

where ρ is the tissue density (kg/m^3), C is the heat capacity of tissue (J/kg $^{\circ}$C), k is thermal conductivity of tissue (W/m $^{\circ}$C), T is the tissue temperature ($^{\circ}$C), T_b is the temperature of blood ($^{\circ}$C), ρ_b is the density of blood (kg/m^3), C_b is the specific heat capacity of blood (J/kg $^{\circ}$C), ω_b is the blood perfusion rate (1/s), Q_{met} is the metabolism heat source (W/m^3) and Q_{ext} is the external heat source term (electromagnetic heat-source density) (W/m^3).

The heat conduction between tissue and blood flow is approximated by the blood perfusion term, $\rho_b C_b \omega_b (T_b - T)$. The external heat source term is equal to the resistive heat generated by electromagnetic field (electromagnetic power absorbed), which is defined as:

$$Q_{ext} = \frac{1}{2} \sigma_{\text{tissue}} \left|\vec{\text{E}}\right|^2 = \frac{\rho}{2}. \text{SAR} \tag{17}$$

Where $\sigma_{tissue} = 2\,\pi f \varepsilon'_r \varepsilon_0$

2.5.1. Boundary condition for heat transfer analysis

The heat transfer is only taking place inside the breast layers, not anywhere else around the model. Fig. 4 shows the assumption (3), a thermal insulation applied on the breast model:

$$n \cdot (k \nabla T) = 0 \tag{18}$$

It is assumed, there is no contact resistance in between the breast model layers. Hence, internal boundaries are continuous:

$$\nabla T_u = \nabla T_d \tag{19}$$

$$n \cdot (k_u \nabla T_u - k_d \nabla T_d) = 0 \tag{20}$$

3. Results and discussions

3.1. Tumor detection

Fig. 5(a) shows the reflection coefficient of the antenna for with and without tumor in the breast model at one position during the scanning. It can be seen that in the presence of the tumor the reflection coefficient is significantly low [18]. All the reflection coefficient at all antenna positions are collected and imported in MATLAB. CMI algorithm is applied on the S11 signals (section 2.2) and a 2D image of the breast is reconstructed, as shown in Fig. 5(b). The red rectangle region with the maximum intensity shows the presence of the embedded tumor in the breast. It can be seen the algorithm is able to reconstruct a good quality image of the tumor embedded in the breast model.

3.2. Effect of tumor distance on the antenna's capability of detecting them

Antenna's capability to detect tumors of different sizes placed at different distances is tested. For that three sizes of tumors at three different distances from the antenna are placed in the breast. The size of three tumors and the three positions they are placed at are mentioned in Tables 3 and 4, respectively. Each tumor from Table 3 is placed at three distances mentioned in Table 4 from the antenna. The antenna scans the breast tissue and the reflection coefficients are collected. Dielectric properties of the breast are taken from Table 5. Fig. 6 shows the reflection coefficients at one antenna position during the scanning. Fig. 6(a) shows reflection coefficient for Tumor 1 placed at three distances. Fig. 6(b) shows the reflection coefficient for Tumor 2 and Fig. 6(c) for Tumor 3. In all three cases, reflection coefficient in presence of the tumor are low in comparison to when tumor was absent in the breast (Fig. 5(a)). Tumor 1 and Tumor 2 shows lowest value of reflection coefficient when the tumors are at 6.2 mm distance from the antenna. Whereas Tumor 3 shows lowest value of reflection coefficient when the tumor is at 8.2 mm distance. Hence, it is observed the antenna is capable of

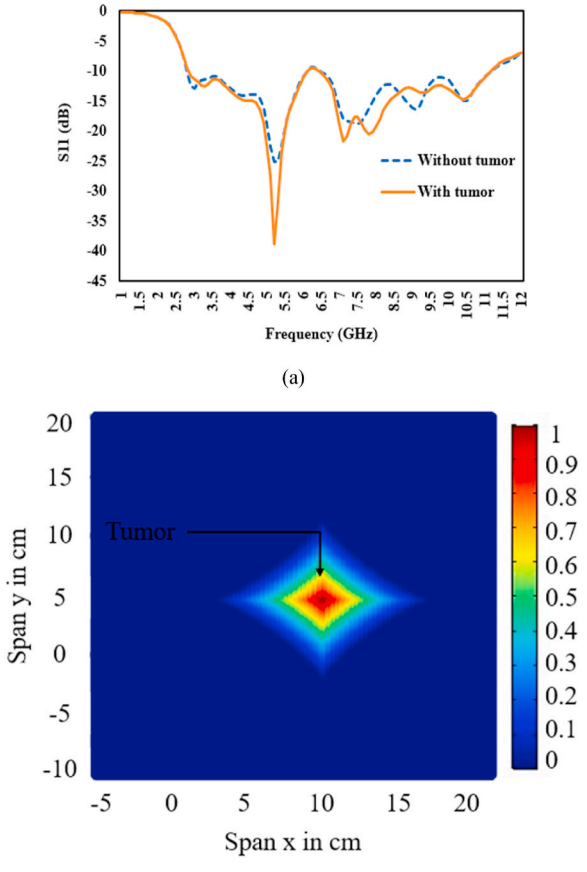

Fig. 5. (a) Reflection coefficient for with and without tumor recorded at one position of the antenna during the scanning, (b) reconstructed 2D-image of the breast.

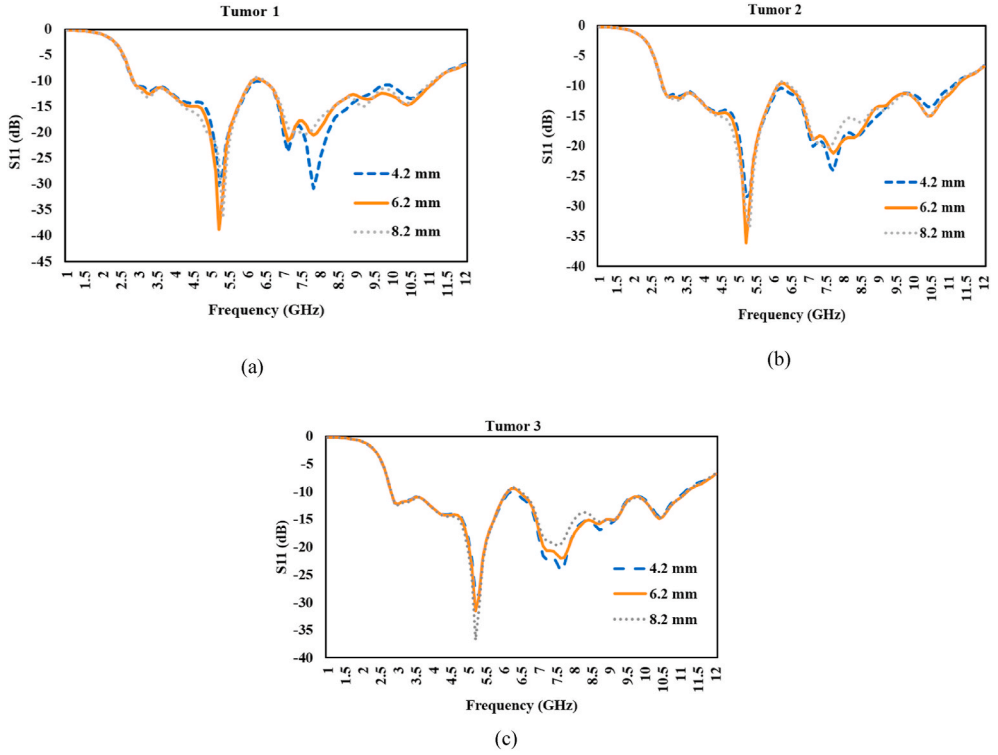

Fig. 6. S11 for tumor at three different sizes, placed at three different distances.

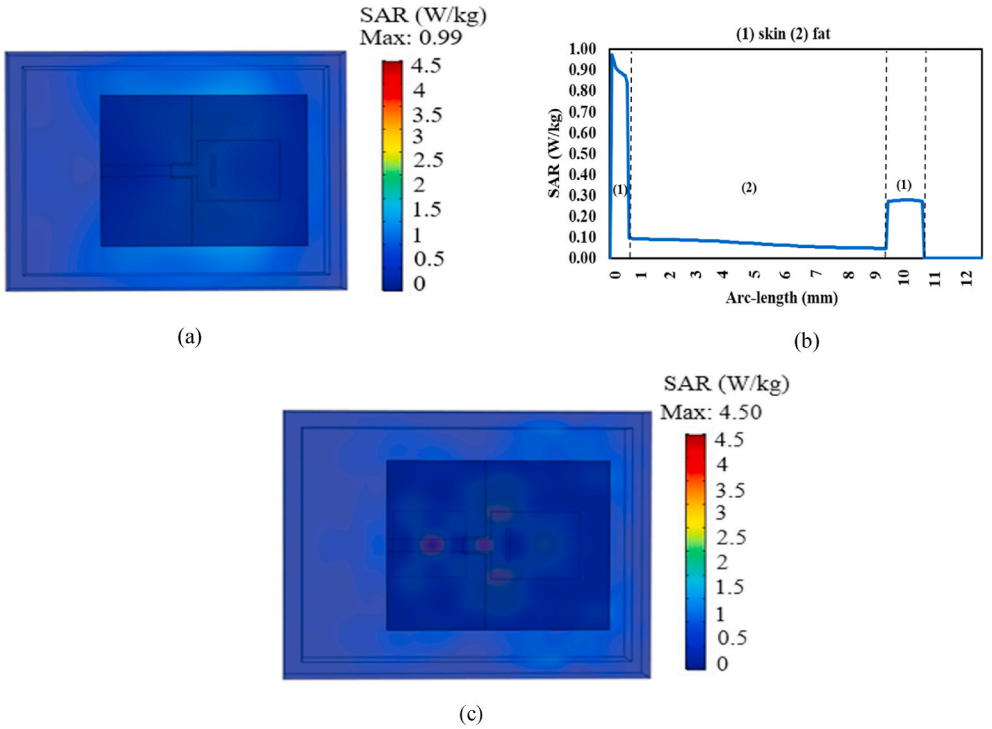

Fig. 7. (a) SAR distribution in the breast model without tumor, (b) SAR distribution inside the breast layers along the arc-length, (c) SAR distribution in the breast model with tumor.

sensing the presence of the tumor as far as 8.2 mm inside the breast model.

3.3. SAR in the tumor for different age group and different frequencies

The part of the EM waves which travels inside the breast tissues gets attenuated and absorbed. The absorbed power in the layers of the breast tissues are calculated by using Equ. 15 for SAR. Fig. 7 (a) and (b) shows the SAR calculation in the breast model in the absence of the tumor exposed to the antenna radiation. Fig. 7(a) shows the SAR distribution in the 3D model of the breast. Whereas, Fig. 7(b) shows the SAR distribution inside the breast layers across an arc-length. As can be seen, the highest value of SAR 0.99 W/kg is found in the skin layer of the breast, region near to the antenna. The SAR then decreases as it goes deeper into the layers of the breast and far from the antenna. The maximum SAR calculated is well below the safety levels, hence, makes the antenna suitable for the MI system [20]. Fig. 7(c) shows the SAR distribution in the breast model in presence of the tumor. Comparison of the SAR in the breast tissues in the presence of a normal and cancerous tumor is studied. The dielectric properties of both types of tumor based on different age group of women (45,47,49, and 51) are taken from Table 6.

Fig. 8 shows the SAR inside the breast layers along an arc-length when a normal and cancerous tumor are inserted in between the fat layer. Both the tumor drastically increases the SAR in the breast. The cancerous tumor shows higher value of SAR (2.46 W/kg) than the normal tumor (1.15 W/kg). The higher value of SAR in the tumors then increases the SAR in the further layers i.e. fat and skin in comparison to when there was no tumor inside the breast (Fig. 7(b)). The energy absorbed by the tumor plays a role in the overall absorption of the energy by the next layers. The higher energy absorption in the cancerous tumor adds upon to the skin and fat layer making them absorb more radiation than before. Women of age group 51 has maximum value of SAR in the breast layers: 0.59 W/kg in skin, 2.46 W/kg in tumor, and 2.60 W/kg in fat. The higher value of electrical conductivity in age 51 of women contribute to more absorption of EM radiation that increases the SAR value in the breast layers.

To further study the effect of dielectric properties on the SAR, three types of tumor (normal, benign, and cancerous) having dielectric properties based on three different frequencies (4,6, and 8 GHz) are included (Table 7). Fig. 9 shows the SAR calculated inside the breast layer along an arc length for the three tumors. It can be seen, at all frequencies, SAR in the cancerous tumor always has higher value than benign and normal tumors. Dielectric properties at 4 GHz frequency causes maximum value of SAR in the cancerous tumor. 3D model of the SAR distribution in the breast for 4 GHz is shown in Fig. 7(c). Hence, it is noted that the SAR distribution in the breast layers highly depends on their dielectric properties and can also be used as a parameter in detecting the tumor position in the breast.

3.4. Temperature distribution in the cancerous tumor

Heat transfer in the breast tissue exposed to microwave radiation from the antenna is also studied. The coupled model of electromagnetic wave propagation and bioheat transfer is analyzed to see the increment in the temperature. The microwave radiation from the antenna travels inside the breast and gets absorbed. The waves attenuate as they go deeper. The absorbed radiation or energy in the tissue layers then gets transformed into thermal energy which increases the overall temperature of the breast. Fig. 10(a) and (b) shows the temperature increase in the breast first in the absence and then in the presence of the cancerous tumor for an exposure time of 60 min, respectively. The maximum temperature increases in the breast in absence of the tumor is 37.055 °C and in the presence of the tumor is 37.095 °C. Fig. 10 (c) and (d) shows the temperature distribution in the breast layers along an arc-length for different exposure time. As can be seen, the temperature in the breast layers in the presence of cancerous tumor (Fig. 10(d)) has higher value of temperature increase in all layers in comparison to when the tumor is absent (Fig. 10(c)). It is observed that the temperature increase inside the breast layers follows the SAR distribution. Just like SAR, the maximum temperature increases were found in the cancerous tissue in the breast. Higher value of electrical conductivity leads to more absorption of radiation which then leads to more increment in the temperature. Also, the metabolic heat generation of the tumor is much higher than the skin and fat which makes the temperature increase in it higher. The blood perfusion rate of skin layer is also higher than the fat and tumor which transfers the energy more rapidly and gets lower increment in the temperature in comparison to fat and tumor.

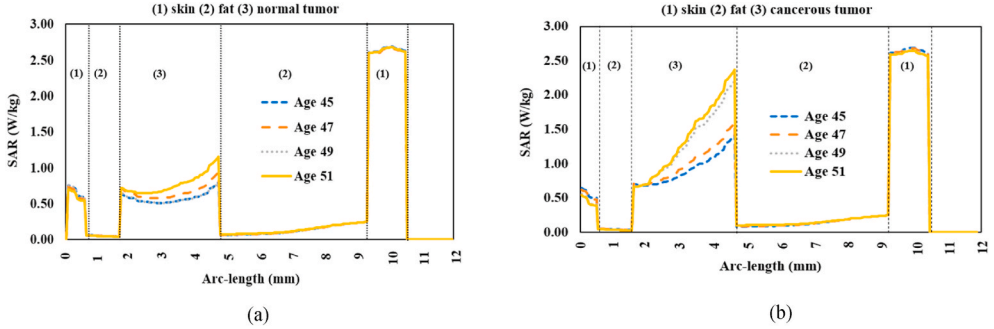

Fig. 8. SAR calculation in different age group of breast model having (a) normal tumor, (b) cancerous tumor.

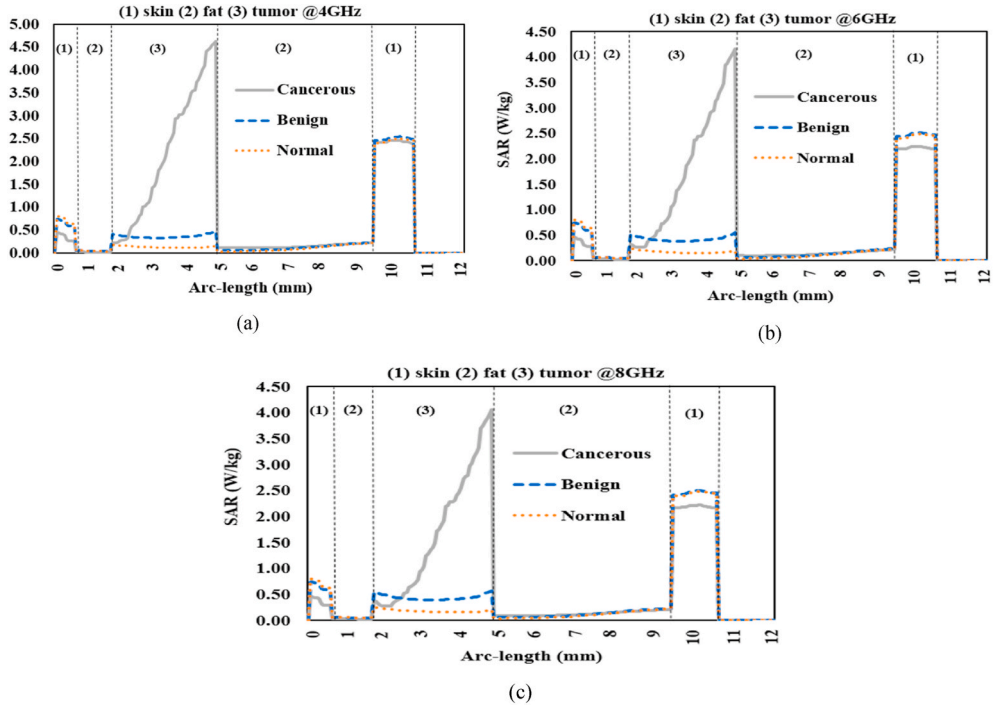

Fig. 9. SAR calculation in the breast model for tumors having dielectric properties for (a) 4 GHz, (b) 6 GHz, and (c) 8 GHz frequencies.

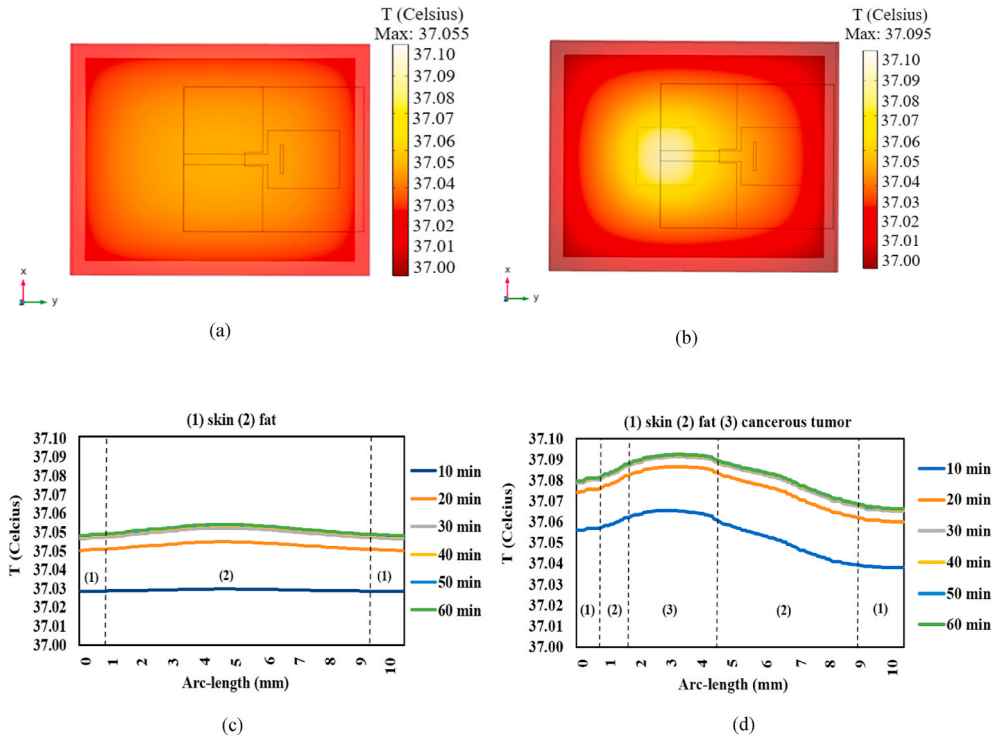

Fig. 10. Temperature distribution in the breast model for (a) without tumor, (b) with tumor, (c) inside breast layers for different exposure time along arc-length without tumor, (d) inside breast layers for different exposure time along arc-length with tumor.

4. Conclusion

The paper proposes a MI system for breast cancer detection by using a wide-band microstrip patch antenna. The antenna collects the reflection coefficients after scanning the breast model at 77 positions. The scanning is performed two times. First in the presence and then in the absence of the tumor. The results obtained from the particular cases shows that the reflection coefficients in presence of the tumor has a lower value in comparison to when the tumor was absent in the breast model. These reflection coefficients collected from both the cases are then imported into MATLAB and processed through the CMI algorithm. It was observed that the presence of the tumor showed a higher peak in the signals. Synesthetic focusing is applied at the end of the algorithm and a 2D image of the breast showing a bright red region where the tumor is present is generated. The antenna is capable of detecting a smallest size of tumor ($6 \times 6 \times 2.4$) mm situated at a distance of 8.2 mm from the antenna. Dielectric properties for different types of tumor and for different age group of patients are included in the study. A coupled model of electromagnetic wave propagation and bio heat transfer is studied to calculate the absorbed power and heat generated in the breast tissues. It is observed that cancerous tumor always absorbs more electric energy which increases the SAR in the breast tissues. This absorbed energy then converts into thermal energy increasing the temperature in the breast model. The dielectric and thermal properties of the breast model highly influence the SAR and temperature. Cancerous tumor has a higher value of electrical conductivity which absorbs more energy in comparison to other tissues of the breast, causing higher SAR and temperature. The temperature increase is found to be correlated with the SAR. The blood perfusion rate of the skin is higher which transfers the absorbed energy at a higher speed to the fat and tumor leading to less temperature increase in the skin layer.

Author statement

Deepshikha Bhargava: Conceptualization, Validation, Investigation, Writing-Original draft preparation.
Phadungsak Rattanadecho: Supervision, Funding acquisition, Project administration.

Declaration of competing interest

The authors declare that they have no known competing financial interests or personal relationships that could have appeared to influence the work reported in this paper.

Acknowledgment

This research was supported by the Thailand Science Research and Innovation Fundamental Fund, the Program Management Unit for Human Resources & Institutional Development, Research and Innovation, NXPO [grant number B05F640205] and NRCT Distinguished Research Professor Grant and Post Doctoral Scholarship.

References

[1] W.H.O.https://www.who.int/news-room/fact-sheets/detail/breast cancer#:~:text=In%202020%2C%20there%20were%202.3,the%20world's%20most%20prevalent%20cancer.
[2] M. Kriege, C.T.M. Brekelmans, C. Boetes, et al., Efficacy of MRI and mammography for breast-cancer screening in women with a familial or genetic predisposition, N. Engl. J. Med. 351 (5) (2004) 427–437.
[3] E.C. Fear, X. Li, S.C. Hagness, et al., Confocal microwave imaging for breast cancer detection: localization of tumors in three dimensions, IEEE (Inst. Electr. Electron. Eng.) Trans. Biomed. Eng. 49 (8) (2002) 812–822.
[4] A.H. Golnabi, P.M. Meaney, S. Geimer, et al., Microwave imaging for breast cancer detection and therapy monitoring, in: IEEE Topical Conference on Biomedical Wireless Technologies, Networks, and Sensing Systems, 2011, pp. 59–62.
[5] F.M. Eltigani, M.A.A. Yahya, M.E. Osman, Microwave imaging system for early detection of breast cancer, in: International Conference on Communication, Control, Computing and Electronics Engineering, ICCCCEE), 2017, pp. 1–5.
[6] P.T. Huynh, A.M. Jarolimek, S. Daye, The false-negative mammogram, Radiographics 18 (5) (1998) 1137–1154, quiz 1243-4, Sep-Oct.
[7] R. Solimene, A. Cuccaro, G. Ruvio, et al., Beamforming and holography image formation methods: an analytic study, Opt Express 24 (8) (2016) 9077–9093, 2016/04/18.
[8] W. Saleh, N. Qaddoumi, Potential of near-field microwave imaging in breast cancer detection utilizing tapered rectangular waveguide probes, Comput. Electr. Eng. 35 (4) (2009) 587–593.
[9] D. O'Loughlin, M. O'Halloran, B.M. Moloney, et al., Microwave breast imaging: clinical advances and remaining challenges, IEEE (Inst. Electr. Electron. Eng.) Trans. Biomed. Eng. 65 (11) (2018) 2580–2590.
[10] T.M. Grzegorczyk, P.M. Meaney, P.A. Kaufman, et al., Fast 3-D tomographic microwave imaging for breast cancer detection, IEEE Trans. Med. Imag. 31 (8) (2012) 1584–1592.
[11] A. Munawar Qureshi, Z. Mustansar, S. Mustafa, Finite-element analysis of microwave scattering from a three-dimensional human head model for brain stroke detection, R. Soc. Open Sci. 5 (7) (2018) 180319.
[12] V. Selvaraj, D. Baskaran, P.H. Rao, et al., Breast tissue tumor analysis using wideband Antenna and microwave scattering, IETE J. Res. (2018) 1–11.
[13] A. M. Abbosh, B. Mohammed, and K. Bialkowski, "Differential Microwave Imaging of Breast Pair for Tumor Detection." pp. 63-64.
[14] N. Niranjan kumar, B.S. Srikanth, S.B. Gurung, et al., A slotted UWB monopole antenna with truncated ground plane for breast cancer detection, Alex. Eng. J. (2020) 1–14.
[15] A.R. Celik, M.B. Kurt, Development of an ultra-wideband, stable and high-directive monopole disc antenna for radar-based microwave imaging of breast cancer, J. Microw. Power Electromagn. Energy 52 (2) (2018) 75–93.
[16] Nasir Iqbal, Saeid Karamzadeh, UWB microstrip antenna design for microwave imaging system, nt. J. Electron. Mech. Mechatron. Eng. 7 (2) (2017) 1411–1417.
[17] R. Inum, M. Rana, K.N. Shushama, et al., EBG based microstrip patch antenna for brain tumor detection via scattering parameters in microwave imaging system, Int. J. Biomed. Imag. 2018 (2018) 1–12.
[18] G. Kaur, A. Kaur, Breast tissue tumor detection using "S" parameter analysis with an UWB stacked aperture coupled microstrip patch antenna having a " + " shaped defected ground structure, Int. J. Microw.Wireless Technol. 12 (7) (2020) 635–651.
[19] A. Hossain, M.T. Islam, A.F. Almutairi, et al., An octagonal ring-shaped parasitic resonator based compact ultrawideband Antenna for microwave imaging applications, Sensors 20 (5) (2020) 1354.

[20] D. Bhargava, N. Leeprechanon, P. Rattanadecho, et al., Specific absorption rate and temperature elevation in the human head due to overexposure to mobile phone radiation with different usage patterns, Int. J. Heat Mass Tran. 130 (2019) 1178–1188.
[21] T. Wessapan, S. Srisawatdhisukul, P. Rattanadecho, Numerical analysis of specific absorption rate and heat transfer in the human body exposed to leakage electromagnetic field at 915 MHz and 2450 MHz, J. Heat Tran. 133 (5) (2011).
[22] T. Wessapan, P. Rattanadecho, Specific absorption rate and temperature increase in human eye subjected to electromagnetic fields at 900 MHz, J. Heat Tran. 134 (9) (2012), 091101-091111.
[23] I. Amdaouch, O. Aghzout, A. Naghar, et al., Breast tumor detection system based on a compact, UWB Antenn. Des. 64 (2018) 123–133.
[24] S. Subramanian, B. Sundarambal, D. Nirmal, Investigation on simulation-based specific absorption rate in ultra-wideband Antenna for breast cancer detection, IEEE Sensor. J. 18 (24) (2018) 10002–10009.
[25] Y. Zhou, C. Herman, Optimization of skin cooling by computational modeling for early thermographic detection of breast cancer, Int. J. Heat Mass Tran. 126 (2018) 864–876, 2018/11/01/.
[26] S.M. Chouiti, L. Merad, S.M. Meriah, et al., An efficient image reconstruction method for breast cancer detection using an ultra-wideband microwave imaging system, Electromagnetics 36 (4) (2016) 225–235.
[27] G. Bindu, S.J. Abraham, A. Lonappan, et al., Detection of dielectric contrast of breast tissues using confocal microwave technique, Microw. Opt. Technol. Lett. 48 (6) (2006) 1187–1190.
[28] V.V. Komarov, Handbook of Dielectric and Thermal Properties of Materials and Microwave Frequencies, 2012.
[29] Y. Cheng, M. Fu, Dielectric properties for non-invasive detection of normal, benign, and malignant breast tissues using microwave theories, Thorac. Cancer 9 (4) (2018) 459–465. Apr.
[30] S.M. Chouiti, L. Merad, S.M. Meriah, et al., Monostatic imaging of an embedded object using a confocal algorithm, Int. J. Numer. Model. Electron. Network. Dev. Field. 31 (5) (2018) e2338.
[31] A. Cuccaro, A. Dell'Aversano, G. Ruvio, et al., Incoherent radar imaging for breast cancer detection and experimental validation against 3D multimodal breast phantoms, J. Imag. 7 (2) (2021), 23.
[32] J.-P. Berenger, A perfectly matched layer for the absorption of electromagnetic waves, J. Comput. Phys. 114 (2) (1994) 185–200.
[33] V. Stanković, D. Jovanović, D. Krstić, et al., Temperature distribution and Specific Absorption Rate inside a child's head, Int. J. Heat Mass Tran. 104 (2017) 559–565.
[34] B. Kundu, D. Dewanjee, A new method for non-Fourier thermal response in a single layer skin tissue, Case Stud. Therm. Eng. 5 (2015) 79–88.